Ising spin glasses in dimension five

P. H. Lundow
Department of Mathematics and Mathematical Statistics, Umeå University, Umeå SE-901 87, Sweden

I. A. Campbell
Laboratoire Charles Coulomb (L2C), UMR 5221 CNRS-Université de Montpellier, Montpellier, France
(Received 15 June 2016; revised manuscript received 28 October 2016; published 10 January 2017)

Ising spin-glass models with bimodal, Gaussian, uniform, and Laplacian interaction distributions in dimension five are studied through detailed numerical simulations. The data are analyzed in both the finite-size scaling regime and the thermodynamic limit regime. It is shown that the values of critical exponents and of dimensionless observables at criticality are model dependent. Models in a single universality class have identical values for each of these critical parameters, so Ising spin-glass models in dimension five with different interaction distributions each lie in different universality classes. This result confirms conclusions drawn from measurements in dimension four and dimension two.

DOI: 10.1103/PhysRevE.95.012112

I. INTRODUCTION

The statistical physics of second-order transitions has been intensively studied in standard systems exemplified by pure ferromagnets, and a thorough understanding of the critical behavior has been reached based on renormalization group (RG) theory. RG theory provides an elegant explanation of the universality of critical exponents, which is the property that all systems within the same universality class (determined only by the physical dimension d and the spin dimension N) have identical values for each critical exponent and for characteristic dimensionless critical parameters. It has been implicitly or explicitly assumed that in spin glasses the form of the interaction distribution is not a relevant parameter for the determination of the universality class, so that, in particular, all Ising spin glasses (ISGs) in a given dimension are expected to have the same critical exponents and critical parameters. The ISG situation is, in fact, much less clear-cut; it has been stated that a fundamentally different theoretical approach to transitions is required [1–5]. Our "working hypothesis" is that the standard RG rules relating exponents hold for each ISG model independently and we then check whether the law of universality among models holds. The scaling rules are discussed in detail in Ref. [6] from the finite-size scaling point of view, and in Ref. [7] from the high-temperature series expansion (HTSE) thermodynamic limit point of view.

We have found from numerical studies on ISGs in dimensions 4 and 2 having bimodal and Gaussian interaction distributions [8–10] that the critical exponents and the critical values for dimensionless constants are not identical for the two models in a given dimension but that they vary with the interaction distribution. It was concluded that the universality class of an ISG depends not only on the physical dimension of the system but also on the form of the interaction distribution.

Here numerical simulation data on ISGs in dimension 5 are presented and analyzed. We are aware of no analogous simulation measurements on ISGs in dimension 5, but some of the present measurements can be compared to results on the same models obtained from the HTSE technique [11,12]. Again, as in dimensions 4 and 2 the values for critical dimensionless constants and for the critical exponents are found to vary with the form of the interaction distribution, confirming that the nonuniversality conclusion reached for ISGs can be generalized.

Dimension 5 is close to the ISG upper critical dimension $d = 6$. For reference, the ϵ-expansion ISG exponent values to leading order in $\epsilon = 6 - d$ [13] are $\gamma = 1 + (6 - d)$, $\nu = 1/2 + 5(6 - d)/12$, and $\eta = -(6 - d)/3$, so for dimension 5 the leading-order exponent values are $\gamma = 2$, $\nu = 11/12 \approx 0.92$, and $\eta = -1/3 \approx -0.33$. The terms of higher order in ϵ are strong and no summations over all terms are known. There are no interaction-distribution-dependent terms in the standard ϵ-expansion expressions but hierarchical spin-glass calculations [1–5] show that the numerical values of the ϵ-expansion coefficients depend on the disorder distribution. The leading-order ϵ-expansion exponent values are all in rough agreement with, but are about 25% stronger than, the range of numerical estimates for the five-dimensional (5D) ISG exponents given below in the Conclusion (Table I), where, for instance, the γ estimates run from 1.73(2) for the bimodal interaction model to 1.49(2) for the Laplacian interaction model.

II. HISTORICAL NOTE

In 1894 Van der Waals introduced the concept of critical exponents, in the context of transitions in liquids; he derived values for the exponents in terms of what is now called a mean-field theory [14]. His student Verschaffelt made very precise experimental measurements on capillarity and in 1900 published experimental estimates for the exponents which were not equal to the mean-field values [15]. His results were ignored for 60 years because they had no theoretical support (see Ref. [16] for an excellent historical account). The situation changed only with Onsager's analytic proof of non-mean-field exponent values in the 2D Ising model [17], which finally led on to the establishment of the principle of universality, within the RG theory concept [18].

Verschaffelt employed temperature-dependent effective exponents in his analyses. Effective exponent analyses were

TABLE I. Estimates of the critical inverse temperatures, exponents, and critical dimensionless parameters β_c, γ, ν, η, $g(\beta_c)$, $\xi/L(\beta,L)$, $h(\beta,L)$, $W_q(\beta,L)$ and for 5D bimodal, uniform, Gaussian, and Laplacian distribution ISG models.

Model	Bimodal	Uniform	Gaussian	Laplacian
Kurtosis	1	1.8	3	6
colrule β_c	0.3885(5)	0.4000(5)	0.4190(5)	0.455(1)
γ	1.73(2)	1.625(20)	1.600(5)	1.49(2)
ν	0.77(2)	0.72(1)	0.720(5)	0.69(1)
η	−0.25(3)	−0.26(3)	−0.22(2)	−0.21(2)
$g(\beta_c)$	0.35(1)	0.294(1)	0.300(5)	0.265(5)
$\xi/L(\beta_c)$	0.450(5)	0.42(1)	0.425(3)	0.401(3)
$P_W(\beta_c)$	1.415(10)	1.425(5)	1.425(10)	1.438(4)
$P_{\text{skew}}(\beta_c)$	1.41(1)	1.422(10)	1.422(10)	1.442(2)
$W_q(\beta_c)$	0.155(5)	0.125(2)	0.128(2)	0.115(3)
$h(\beta_c)$	0.267(5)	0.235(3)	0.228(3)	0.196(5)

reintroduced much later for experimental [19] and numerical [7,20] ferromagnetic data. Below we also will use effective exponents in the analysis of ISG simulation data.

III. SIMULATION MEASUREMENTS

We are aware of no previous publications of precise simulation data on ISGs in dimension 5. The standard ISG Hamiltonian is

$$\mathcal{H} = -\sum_{ij} J_{ij} S_i S_j, \tag{1}$$

with the nearest-neighbor symmetric distributions normalized to $\langle J_{ij}^2 \rangle = 1$. The normalized inverse temperature is $\beta = (\langle J_{ij}^2 \rangle / T^2)^{1/2}$. The Ising spins live on simple hypercubic lattices with periodic boundary conditions. The spin overlap parameter is defined, as usual, by

$$q = \frac{1}{L^d} \sum_i S_i^A S_i^B, \tag{2}$$

where A and B indicate two copies of the same system. The link overlap is defined analogously as

$$q_l = \frac{1}{dL^d} \sum_{ij} S_i^A S_j^A S_i^B S_j^B, \tag{3}$$

where the sum is taken over the edges ij in the underlying graph. We have studied the symmetric bimodal ($\pm J$), Gaussian, uniform $[P(J) = 1/[2 \times 3^{1/2}]$ for $-3^{1/2} < J < 3^{1/2}]$ and Laplacian $P(J) = 2^{1/2} \exp(-2^{1/2}|J|)$ distribution ISG models in dimension 5. The principles of the data analysis are the same as for studies on ISG models in dimensions 3 and 4.

The simulations were carried out using the exchange Monte Carlo method for equilibration using so-called multispin coding, on 2^{12} individual samples at each size from $L = 3$ to $L = 10$ for the bimodal and Gaussian models. (It can be noted that an $L = 10$ sample in $d = 5$ contains more spins than an $L = 46$ sample in $d = 3$, so the simulations are laborious.) However, see the thermodynamic limit (ThL) figure-of-merit discussion in Sec. VI. For the uniform distribution model 2^{12} samples were studied up to $L = 6$, and 2^9 samples up to $L = 9$, and for the Laplacian model 2^{12} samples were studied up to $L = 6$, and 2^9 samples up to $L = 8$. An exchange was attempted after every sweep with a success rate of at least 30%. At least 40 temperatures were used, forming a geometric progression reaching a maximum $\beta = 0.41$ in the bimodal model, $\beta = 0.44$ in the Gaussian model, $\beta = 0.47$ in the uniform model, and $\beta = 0.52$ in the Laplacian model. This ensures that our data span the critical temperature region which is essential for the finite-size scaling (FSS) analyses. Near the critical temperature the β step length was at most 0.003. The various systems were deemed to have reached equilibrium when the sample average susceptibility for the lowest temperature showed no trend between runs. For example, for $L = 10$ this means about 200 000 sweep-exchange steps.

It should be pointed out that there is no single definitive method for determining equilibration in all cases. This can only be based on consistency between repeated experiments. Stability between sample averages of $\langle q^2 \rangle$ at the highest β value for long runs appears to be a strong indicator of equilibration. We simply plot these values versus the number of sweeps and stop the equilibration process when the data appear constant (modulo noise). Note also that we use the values at the largest β value, which is well beyond the β_c value. Thus, we can be confident that in the finite-size scaling regime around β_c, and *a fortiori* in the thermodynamic limit envelope regime with $\beta < \beta_c$, the systems are definitely equilibrated as they are all at lower β and so will have equilibrated faster.

After equilibration, at least 200 000 measurements were made for each sample for all sizes, taking place after every sweep-exchange step. Data were registered for the energy $E(\beta,L)$, the correlation length $\xi(\beta,L)$, for the spin overlap moments $\langle |q| \rangle$, $\langle q^2 \rangle$, $\langle |q|^3 \rangle$, $\langle q^4 \rangle$ and the corresponding link overlap q_ℓ moments. In addition, the correlations $\langle E(\beta,L), U(\beta,L) \rangle$ between the energy and the observables $U(\beta,L)$ were also registered so that thermodynamic derivatives could be evaluated using the thermodynamic relation $\partial U(\beta,L)/\partial\beta = \langle U(\beta,L), E(\beta,L) \rangle - \langle U(\beta,L) \rangle \langle E(\beta,L) \rangle$, where $E(\beta,L)$ is the energy [21].

As a double check for equilibration in the case of Gaussian interactions, we verify that the systems obey the simple rule $[\langle q_l \rangle] + [\langle E \rangle]/\beta = 1$ to within 10^{-4} for large L at all β values measured; this is an equilibration condition suggested in Ref. [22]. This also provides us with an indirect estimate of how many sweeps are required for equilibration for the other interaction cases. In passing, we observe that 5D systems tend to reach equilibration in a more distinct manner than 4D systems do, which, in turn, are considerably easier to equilibrate than 3D systems.

Bootstrap analyses were carried out for the errors in the observables $U(\beta,L)$ as well as in their derivatives. Bootstrapping (the nonparametric version) here refers to the simple and quite general method (some care should be taken when the underlying distribution is heavy tailed) for estimating the error of some statistic through random sampling with replacement. As a simple example, if we have N_s samples (i.e., J_{ij} configurations), each with its own $\langle q^2 \rangle$ and $\langle q^4 \rangle$, then the error in the quantity $[\langle q^4 \rangle]/[\langle q^2 \rangle]^2$ is obtained by randomly choosing with replacement N_s samples, e.g., 1000 times and

compute the resulting $[\langle q^4\rangle]/[\langle q^2\rangle]^2$ for each such choice (i.e., a bootstrap sample). The standard deviation of these values then gives the error estimate $\hat{\sigma}$ of $[\langle q^4\rangle]/[\langle q^2\rangle]^2$.

Note that $\langle|q|\rangle$ and $\langle q^2\rangle$ for each sample are themselves mean values also having variances and standard errors. This point, which is, of course, not specific to dimension 5 but occurs in all analogous ISG studies, is discussed in the Appendix.

IV. FINITE-SIZE SCALING

The usual approach to critical parameter measurements through simulations is to study the size dependence of dimensionless observables $Q(\beta,L)$ [generally the Binder cumulant $g(\beta,L) = (3 - [\langle q^4\rangle]/[\langle q^2\rangle]^2)/2$ and the normalized correlation length $\xi(\beta,L)/L$] in the regime very near the critical point. $g(\beta,L)$ must saturate at $g(\beta,L) = 1$ for $\beta \gg \beta_c$, which is not the case for $\xi(\beta,L)/L$. It can be noted that we find critical $g(\beta_c)$ values much lower in 5D ISGs than in 3D or even in 4D ISGs, so the 5D $g(\beta,L)$ data have space to "fan out" beyond β_c making this parameter more efficient for critical regime analyses in 5D than in the other dimensions. The typical FSS expression, valid in the near critical region if there is a single dominant scaling correction term, is (see [6])

$$Q(\beta,L) = Q_c + AL^{-\omega} + B(\beta - \beta_c)L^{1/\nu}, \tag{4}$$

where ν is the correlation length critical exponent and ω is the exponent of the leading finite-size correction term. For any dimensionless parameter Q the Q_c critical values are identical for all systems within a universality class and the correction exponent ω is universal for all observables. However, when higher-order correction terms are strong the "effective" leading correction exponent obtained from data fits can vary from observable to observable. From the HTSE and ThL data, which we will discuss later, the 5D correction exponent is typically $\omega \approx 1.0$ in the different models.

We will use the finite-size scaling measurements as one method to estimate the critical inverse temperatures β_c, together with the dimensionless parameter values Q_c at criticality extrapolated to the infinite-size limit. The critical exponent ν can be estimated from the derivatives at criticality through [6]

$$\left.\frac{\partial Q(\beta,L)}{\partial\beta}\right|_{\beta_c} = A_Q L^{1/\nu}(1 + a_Q L^{-\omega} + \cdots). \tag{5}$$

The critical exponent η can be estimated through [6]

$$\frac{\chi(\beta_c,L)}{L^2} = A_\chi L^{-\eta}(1 + a_\chi L^{-\omega} + \cdots). \tag{6}$$

For the present analysis we have recorded the FSS behavior of various dimensionless parameters in addition to the Binder cumulant $g(\beta,L)$ and the correlation length ratio $\xi(\beta,L)/L$. The dimensionless parameter $W(\beta,L)$ for Ising ferromagnets was introduced in Ref. [23]. In the ISG context the parameter $W_q(\beta,L)$ is defined by

$$W_q(\beta,L) = \frac{1}{\pi - 2}\left(\frac{\pi\,[\langle|q|\rangle]^2}{[\langle q^2\rangle]} - 2\right). \tag{7}$$

In the same spirit we will also make use of other dimensionless parameters,

$$h(\beta,L) = \frac{1}{\sqrt{\pi} - \sqrt{8}}\left(\sqrt{\pi}\,\frac{[\langle|q^3|\rangle]}{[\langle q^2\rangle]^{3/2}} - \sqrt{8}\right), \tag{8}$$

$$P_W = \left[\frac{\langle|q|\rangle^2}{\langle q^2\rangle}\right], \tag{9}$$

and the skewness

$$P_{\text{skew}} = \left[\frac{\langle|q|^3\rangle}{\langle q^2\rangle^{3/2}}\right], \tag{10}$$

which also have analogous scaling properties.

V. THERMODYNAMIC DERIVATIVE PEAK ANALYSIS

The thermodynamic derivative peak analysis can also be an efficient method for analyzing data in a ferromagnet or an ISG. Near criticality in a ferromagnet, for a number of standard observables Q the heights of the peaks of the thermodynamic derivatives $\partial Q(\beta,L)/\partial\beta$ scale for large L as [21,24]

$$D_{\max}(L) = \left.\frac{\partial Q(\beta,L)}{\partial\beta}\right|_{\max} \propto L^{1/\nu}(1 + aL^{-\omega/\nu}). \tag{11}$$

The observables used for $Q(\beta,L)$ can be, for instance, the Binder cumulant $g(\beta,L)$ or the logarithm of the finite-size susceptibility $\ln[\chi(\beta,L)]$ [21]. Without needing a value of β_c as input, the large L peak height $D_{\max}(L)$ against L plot provides $1/\nu$ directly, to within scaling corrections.

In addition, the temperature location of the derivative peak $\beta_{\max}(L)$ scales as

$$\beta_c - \beta_{\max}(L) \propto L^{-1/\nu}(1 + bL^{-\omega/\nu}). \tag{12}$$

We note that the inverse of the derivative peak height $1/D_{\max}(L)$ and the peak location temperature difference $\beta_c - \beta_{\max}(L)$ are both proportional to $L^{-1/\nu}(1 + aL^{-\omega/\nu} + \cdots)$ (with the leading correction terms having different prefactors). Then $\beta_{\max}(L)$ plotted against $1/D_{\max}(L)$ must tend linearly towards the intercept β_c as $1/D_{\max}(L)$ tends to zero for large L. All plots of the same type for different observables Q should extrapolate consistently to the true β_c. The leading correction is eliminated to first order and, together with the higher-order corrections, only appears as a modification to the straight line for small L. Provided that the peaks for the chosen observable fall reasonably close to β_c, these data can be much simpler to analyze than those from the crossing technique. For ferromagnets, Ferrenberg and Landau [21] found this form of analysis significantly more accurate than the standard Binder cumulant crossing approach.

In the ISG context exactly the same methodology can be used as in the ferromagnet [8,9]. Because the exponent ν is relatively small in 5D ISGs this technique is an efficient independent method for estimating β_c. As far as we are aware this analysis has not been used previously by other authors in ISGs.

VI. THERMODYNAMIC LIMIT SCALING

The high-temperature series expansion for the spin-glass susceptibility of an ISG with a symmetrical interaction

distribution can be written [12]

$$\chi(\beta) = 1 + a_1\beta^2 + a_2\beta^4 + \cdots . \tag{13}$$

Only even terms in powers of β exist because of the symmetry between positive and negative interactions, so β^2, rather than β, is the natural thermal scaling variable [11,12,25,26]. In principle, an infinite set of exact HTSE factors a_n exists. In practice, terms in different ISG models have been calculated, at best, up to $n = 15$ (see Refs. [11,12,25]). Then, according to Darboux's first theorem [27], the asymptotic form of the sum of the entire series (all terms to infinite n) is eventually dominated by the closest singularity to the origin, which in the simplest case is the physical singularity [7,12], so near β_c^2,

$$\chi(\beta) = C_\chi[1 - (\beta/\beta_c)^2]^{-\gamma}, \tag{14}$$

with β_c^2 being the inverse critical temperature squared and γ the standard critical exponent.

It is thus natural to adopt $\tau = 1 - (\beta/\beta_c)^2$ as the scaling variable in analyses of ThL ISG simulation data, as in the HTSE analyses [12,26]. (An equivalent natural scaling variable which has been generally used for HTSE analyses on ISGs with symmetric bimodal interaction distributions is [11,25] $w = 1 - \tanh(\beta)^2/\tanh(\beta_c)^2$. The discussion above holds throughout, with w replacing τ. The exponents, of course, remain the same, though the factors C,a, etc., are modified.) Then the Wegner scaling expression [28] for the ThL ISG susceptibility extended over the whole paramagnetic range is

$$\chi(\tau) = C_\chi\tau^{-\gamma}(1 + a_\chi\tau^\theta + b_\chi\tau^{\theta'} + \cdots), \tag{15}$$

where $\theta = \nu\omega$ is the leading thermal correction exponent and the second term is generally analytic. (The relation between θ and ω follows from a dimensional argument.) In practice, with a finite set of correction terms the expression becomes approximate. The standard RG scaling variable $t = (T - T_c)/T_c$ is often used for ISG simulation analyses close to criticality, but this scaling variable is not convenient at higher temperatures as t diverges at infinite temperature, while τ tends to 1. Also with this scaling variable the temperature appears as T, not T^2, so t is only appropriate for ISGs as an approximation near β_c.

The HTSE second moment of the ISG spin-spin correlations $\mu_2 = \sum r^2\langle S_0.Sr\rangle$ (where r is the distance between the spins situated at positions 0 and r) is of the form (see Ref. [7,29] for the ferromagnetic case)

$$\mu_2(\beta) = \beta^2(z + b_1\beta^2 + b_2\beta^4 + \cdots), \tag{16}$$

where z is the number of nearest neighbors. The ThL μ_2 diverges at β_c as $\tau^{-(\gamma+2\nu)}$. Then, invoking again Darboux's theorem to link the series within the brackets to the critical divergence, the appropriate scaling form can be written as

$$\mu_2(\beta) = C_\mu z\beta^2\tau^{-(\gamma+2\nu)}(1 + a_\mu\tau^\theta + \cdots). \tag{17}$$

As the ThL second moment correlation length is defined through $\mu_2 = z\chi(\beta)\xi(\beta)^2$, the Wegner form for the normalized ISG ThL correlation length can be written [26]

$$\xi(\beta)/\beta = C_\xi\tau^{-\nu}(1 + a_\xi\tau^\theta + b_\xi\tau + \cdots). \tag{18}$$

It is important to note the factor β, which normalizes $\xi(\beta)$ in this equation.

The form of susceptibility scaling outlined here for ISGs was used from the earliest HTSE studies of critical behavior in ferromagnets and then in ISGs [7,11,12,30]. The analogous normalized correlation length form was introduced explicitly in Ref. [26].

The full HTSE sum is by construction in the (infinite L) ThL, but extrapolations from high temperature must be made in order to estimate behavior at criticality, because the complete series is not available [12]. Simulation data are necessarily taken at finite L, but can be considered as also being in the ThL as long as $L \gg \xi(\beta)$, where $\xi(\beta)$ is the ThL correlation length. The ThL envelope curves can generally be recognized by inspection of the data plots. As a rule of thumb, the condition $L > 6\xi(\beta)$ can generally be taken as sufficient, with observables independent of L and equal to the ThL values as long as this condition is satisfied. The simulation data supplement and extend the HTSE data. As $\xi(\beta) \sim \beta[1 - (\beta/\beta_c)^2]^{-\nu}$ in ISGs, the ThL condition can be written approximately in terms of a figure of merit; if $\tau_{\min}$ is the lowest reduced temperature to which the ThL condition holds for size L,

$$\tau_{\min} \approx (L/6\beta_c)^{-1/\nu}. \tag{19}$$

In dimension 5 with $\beta_c \approx 0.4$ and $\nu \approx 0.7$ the condition implies $\tau_{\min} \approx 0.15$ if the largest size used is $L = 10$. This $\tau_{\min}$ corresponds to a temperature within 8% of the critical temperature. It can be underlined that in dimension 3 with the appropriate parameters for ISGs, $\beta_c \approx 1$, $\nu \approx 2.5$, to reach $\tau_{\min} \approx 0.15$ would require sample sizes to $L \approx 300$, far beyond the maximum sizes which have been studied numerically up to now in 3D ISGs. The ISG ThL regime can be studied numerically reasonably close to criticality in dimension 5 (and dimension 4) but the situation is much more delicate in dimension 3.

Temperature- and size-dependent susceptibility and correlation length effective exponents, valid over the entire paramagnetic regime, can be defined by

$$\gamma(\tau,L) = -\partial \ln \chi(\tau,L)/\partial \ln \tau, \tag{20}$$

$$\nu(\tau,L) = -\partial \ln[\xi(\tau,L)/\beta]/\partial \ln \tau. \tag{21}$$

The critical limits are $\gamma(0,\infty) = \gamma$ and $\nu(0,\infty) = \nu$; extrapolations must be made to estimate the critical exponents from HTSE or simulation data. In simple hypercubic lattices of dimension d, where $z = 2d$, the exact ISG high-temperature limits for all L are $\gamma(1,L) = 2d\beta_c^2$ and $\nu(1,L) = (d - K/3)\beta_c^2$, where K is the kurtosis of the interaction distribution ($K = 1$ for the bimodal distribution, $K = 3$ for the Gaussian distribution, $K = 9/5$ for the uniform distribution, and $K = 6$ for the Laplacian distribution).

The value of β_c enters implicitly into the definitions of $\gamma(\tau,L)$ and $\nu(\tau,L)$ in Eq. (21) through the definition of τ, so it is important to have well-established estimates for β_c for the γ and ν effective exponent analyses.

Turning to the exponent η, the temperature-dependent effective $\eta(\beta,L)$ can be estimated through

$$2 - \eta(\beta,L) = \frac{\partial \ln \chi(\beta,L)}{\partial \ln[\xi(\beta,L)/\beta]} = \frac{\gamma(\beta,L)}{\nu(\beta,L)}. \tag{22}$$

Alternatively, one can make a log-log plot of $y(\beta,L) = \chi(\beta,L)/[\xi(\beta,L)/\beta]^2$ against $x(\beta,L) = \xi(\beta,L)/\beta$. At high temperatures and for all L, $x(\beta,L)$ and $y(\beta,L)$ both tend to 1 as β tends to 0. For large L and temperatures near criticality, the slope of the ThL envelope curve $\partial \ln y(\beta,L)/\partial \ln x(\beta,L)$ tends to the critical exponent $-\eta$ in the limit $\beta \to \beta_c$, where both $y(\beta,L)$ and $x(\beta,L)$ diverge. With an appropriate fit function, extrapolation of the ThL envelope curve to the large L limit leads to an estimate for η purely from ThL data, without invoking the FSS estimate for β_c.

VII. PRIVMAN-FISHER SCALING

The Privman-Fisher scaling ansatz [31] for an observable $Q(\beta,L)$ can be written in the simple general form

$$Q(\beta,L)/Q(\beta,\infty) = F[L/\xi(\beta,\infty)], \tag{23}$$

where Wegner thermal correction terms are implicitly included in $Q(\beta,\infty)$ and $\xi(\beta,\infty)$. A leading finite-size correction term can be introduced [32]:

$$\frac{Q(\beta,L)}{Q(\beta,\infty)} = F'[L/\xi(\beta,\infty)]\left\{1 + \frac{G_Q[L/\xi(\beta,\infty)]}{L^{\omega}}\right\}. \tag{24}$$

For given values of the critical inverse temperature and exponents β_c, ν, and η, assuming the leading ThL ISG extended scaling expressions $\chi(\beta,\infty) \propto [1-(\beta/\beta_c)^2]^{-\gamma}$ and $\xi(\beta,\infty) \propto \beta[1-(\beta/\beta_c)^2]^{-\nu}$ are valid and ignoring Wegner correction terms, the basic Privman-Fisher ansatz for the susceptibility can be readily transformed into

$$\frac{\chi(\beta,L)}{(L/\beta)^{2-\eta}} = \mathcal{F}\{|[1-(\beta/\beta_c)^2]|(L/\beta)^{1/\nu}\}, \tag{25}$$

as applied in [26,33]. This extended scaling form is less sensitive to the precise values of the critical parameters than is the ThL scaling and does not contain the correction terms. However, it allows one to scale all the data, not only those from the ThL regime, but also from the crossover regime between the ThL and FSS regimes, from the critical regime, and even from the region to temperatures rather below the critical temperature. Below it will be seen that very acceptable scaling is observed for the data from each of the four models studied, when the appropriate scaling parameters are used. This shows that the data for all L and for all temperatures from infinity down to below T_c can be encapsulated in the scaling expression (25), adjusting only the three critical parameters β_c, ν, and η. If Wegner correction terms have been estimated from ThL scaling, these can be introduced to improve the scaling but their influence will only be felt well outside the critical region.

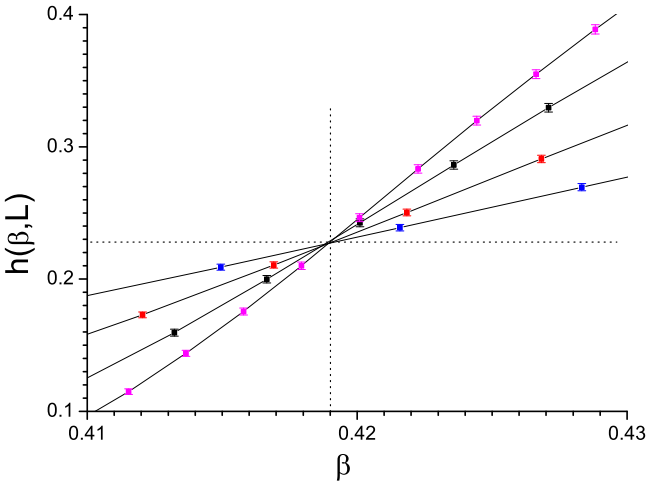

FIG. 2. Gaussian 5D ISG model. Even L data for the observable $h(\beta,L)$ against β, $L = 4$, 6, 8, and 10 (top to bottom on the left).

VIII. THE 5D GAUSSIAN DISTRIBUTION ISG MODEL

For the Gaussian distribution model, the FSS Binder parameter $g(\beta,L)$ data and the parameter $h(\beta,L)$ both happen to show no visible correction to scaling at criticality (Figs. 1 and 2). This provides us with consistent and accurate estimates $\beta_c = 0.4190(3)$, $g_c = 0.300(2)$, and $h_c = 0.225(1)$. The data for the other dimensionless parameters in the form of fixed

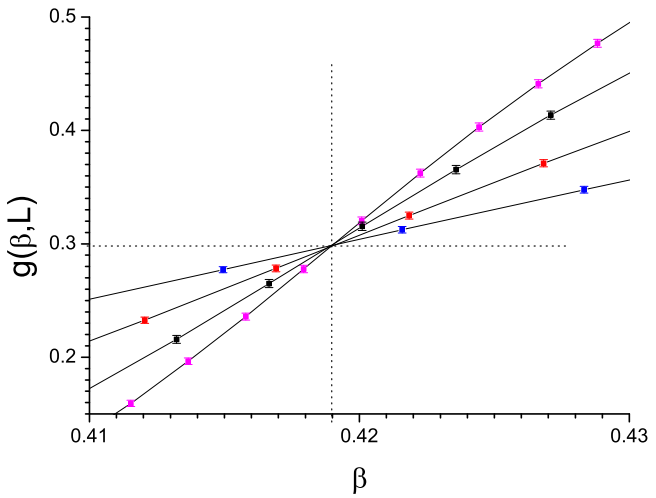

FIG. 1. Gaussian 5D ISG model. Even L Binder cumulants $g(\beta,L)$ against inverse temperature β, $L = 4$, 6, 8, and 10 (top to bottom on the left).

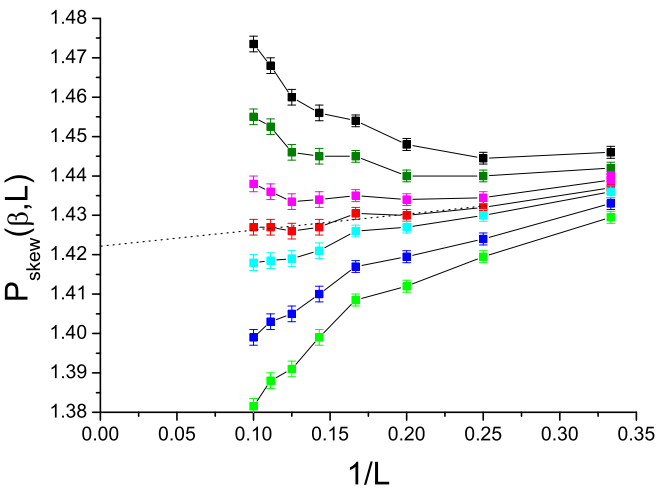

FIG. 3. Gaussian 5D ISG. $P_{\text{skew}}(\beta,L)$ against $1/L$ for fixed β, $\beta = 0.424$, 0.422, 0.420, 0.419, 0.418, 0.416, and 0.414 (top to bottom). Dashed line, estimated criticality.

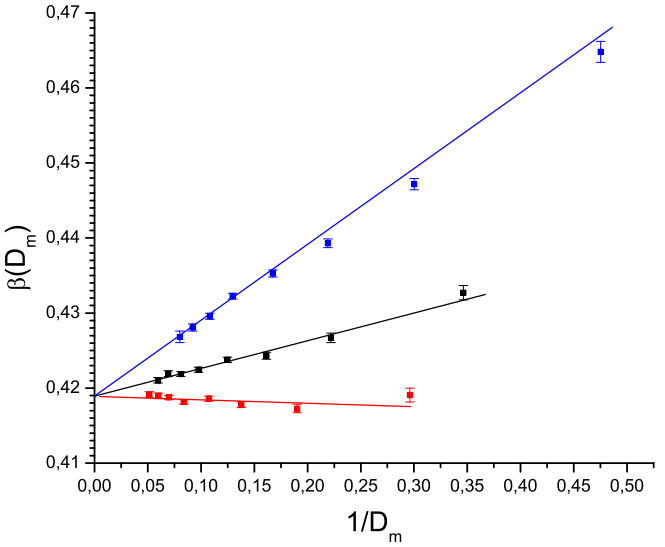

FIG. 4. Gaussian 5D ISG. Peak location $y = \beta_{\max}$ against inverse peak height $x = 1/D_{\max}$ for the derivatives $\partial P_W/\partial\beta$, $\partial h/\partial\beta$, and $\partial g/\partial\beta$ (top to bottom). Sizes $L = 3$, 4, 5, 6, 7, 8, 9, and 10 (increasing to the left). For each observable the points extrapolate to $y(x) = \beta_c$ at the intercept; see text.

temperature plots show only weak corrections to scaling. They are all consistent with $\beta_c = 0.419$ and $\omega \approx 1$. As the finite-size corrections are weak the analyses are rather insensitive to the assumed value for ω; see, for instance, Fig. 3. The critical value estimates for the dimensionless parameters are listed in the Conclusion, (Table I). Data for the locations of thermodynamic derivative peaks are shown in Fig. 4. They are also all consistent with $\beta_c = 0.419$.

The effective exponents $\gamma(\tau,L) = \partial \ln \chi(\tau,L)/\partial \ln \tau$ and $\nu(\tau,L) = \partial \ln[\xi(\tau,L)/\beta]/\partial \ln \tau$, with β_c fixed at 0.419, are shown in Figs. 5 and 6. For Fig. 5 a HTSE curve (calculated with a_n values obtained explicitly from summing the tabulation

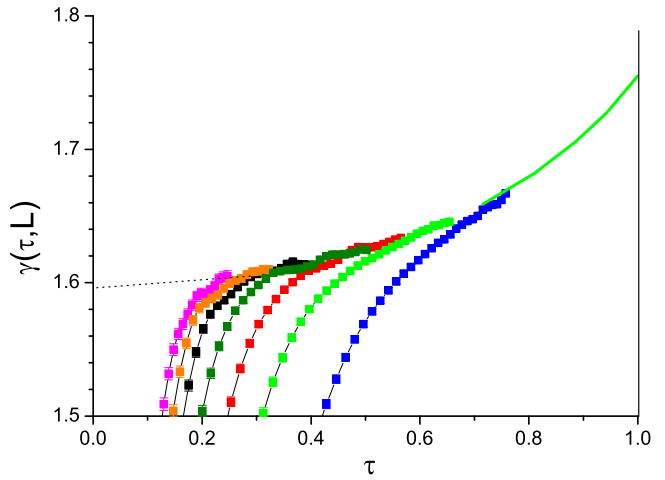

FIG. 5. Gaussian 5D ISG. Effective exponent $\gamma(\tau,L)$ as a function of τ with $\beta_c = 0.419$. Points, simulation data for $L = 10$, 9, 8, 7, 6, 5, and 4 (left to right); dashed curve, fit; continuous (green) curve on the right, calculated by summing the HTSE tabulation of [12].

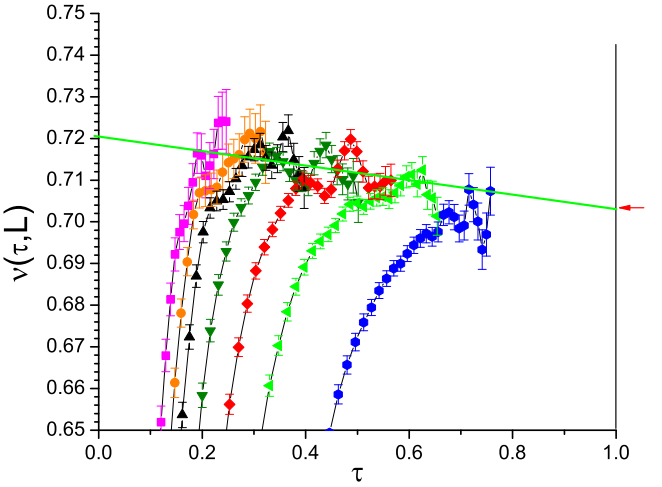

FIG. 6. Gaussian 5D ISG. Effective exponent $\nu(\tau,L)$ as function of τ with $\beta_c = 0.419$. Points, simulation data for $L = 10$, 9, 8, 7, 6, 5, and 4 (left to right); continuous (green) curve, fit.

in [12]) is also included with the simulation data. This curve, calculated with the known 13 leading HTSE terms only, is essentially exact in the high- to moderate-τ region. The numerical data are in excellent agreement with the HTSE curve. The fits to the ThL envelope data correspond to

$$\chi(\tau) = 0.94\tau^{-1.59}(1 + 0.0625\tau^{2.4}), \tag{26}$$

$$\xi(\tau) = 0.98\beta\tau^{-0.72}(1 + 0.017\tau^{2.4}). \tag{27}$$

Thus, the exponent estimates are $\gamma = 1.59(2)$ and $\nu = 0.72(1)$, so $\eta = 2 - \gamma/\nu = -0.20(2)$. In Sec. XII a detailed discussion is given of the Gaussian HTSE estimates of Ref. [12]. For both γ and ν the corrections to scaling in the whole paramagnetic temperature region are weak. For $\chi(\tau)$ the "effective" correction appears to be a sum of high-order correction terms. Any

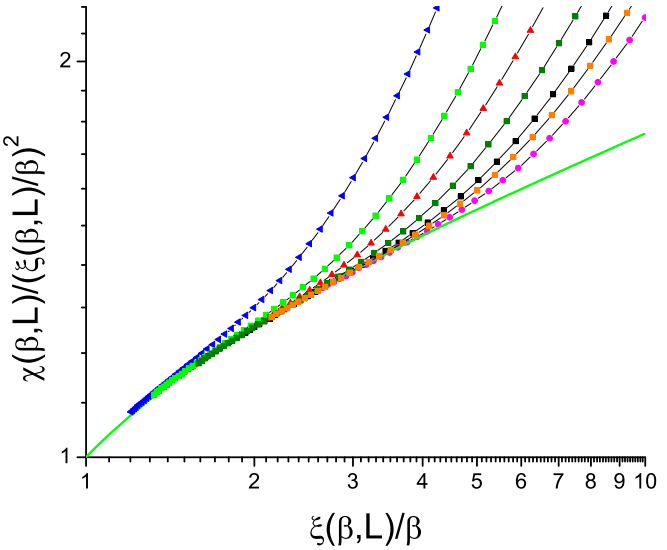

FIG. 7. Gaussian 5D ISG. The ratio $\chi(\beta,L)/[\xi(\beta,L)/\beta]^2$ against $\xi(\beta,L)/\beta$ for $L = 10$, 9, 8, 7, 6, 5, and 4 (right to left). Continuous green curve, fit. No value is assumed for β_c.

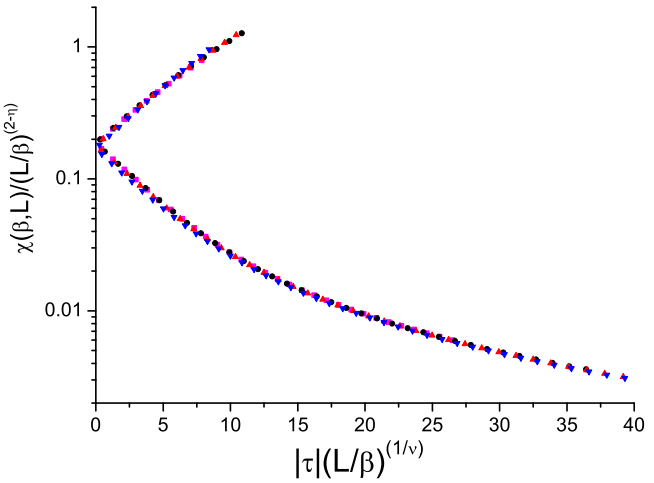

FIG. 8. Gaussian 5D ISG. Privman-Fisher-like scaling of the $\chi(\beta,L)$ data following the form used in [26], with assumed parameters $\beta_c = 0.419$, $\nu = 0.72$, $\eta = -0.19$, and no adjustments. $L = 10$, pink squares; $L = 8$, black circles; $L = 6$, red triangles; $L = 4$, blue inverted triangles. Upper branch, $\beta > \beta_c$; lower branch, $\beta < \beta_c$.

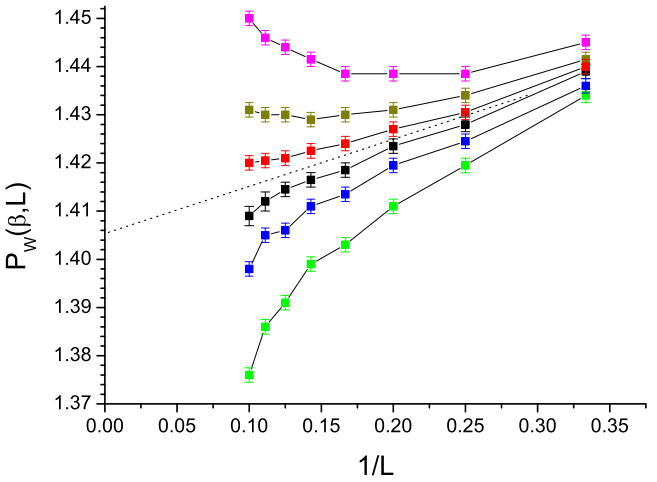

FIG. 10. Bimodal 5D ISG. $P_W(\beta,L)$ against $1/L$ for fixed β, $\beta = 0.385$, 0.387, 0.388, 0.389, 0.390, and 0.392 (top to bottom). $L = 10$, 9, 8, 7, 6, 5, 4, and 3 (left to right). Dashed line, estimated criticality, $\beta = 0.3885$.

correction with $\theta \approx 1$, which might be expected from either the conformal correction or from a leading analytic correction, seems to be negligible.

A log-log plot of $y(\beta,L) = \chi(\beta,L)/[\xi(\beta,L)/\beta]^2$ against $x(\beta,L) = \xi(\beta,L)/\beta$ is shown in Fig. 7. The estimated asymptotic slope of the ThL envelope curve $\partial \ln y(\beta,L)/\partial \ln x(\beta,L)$ gives an estimate for the critical exponent $\eta = -0.19(2)$ without invoking any value for β_c. This η estimate is consistent with the value from the ratio γ/ν.

The basic Privman-Fisher extended scaling (25) for $\chi(\beta,L)$ with these parameter values is shown in Fig. 8. The scaling is excellent (including the range of temperatures below T_c, the upper branch) apart from weak deviations visible for the smallest size $L = 4$, which could be accounted for by a finite-size correction term.

IX. THE 5D BIMODAL DISTRIBUTION ISG MODEL

For this model the dimensionless observable sets all show corrections to finite-size scaling. Data for four standard observables are shown in Figs. 9, 10, 11, and 12. For β_c the best overall estimate is $\beta_c = 0.3885(5)$. Thermodynamic derivative peak location data are shown in Fig. 13. The extrapolations are consistent with the same value, $\beta_c = 0.3885(5)$.

The effective exponents $\gamma(\tau,L)$ and $\nu(\tau,L)$ defined above are shown in Fig. 14 and 15. The high-temperature curve included in Fig. 14 is evaluated from the HTSE series tabulation in Ref. [12]. The critical exponents estimated by

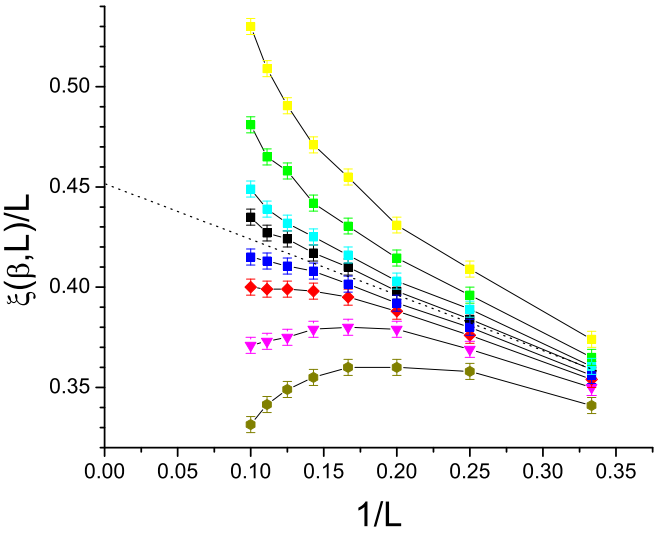

FIG. 9. Bimodal 5D ISG. $\xi(\beta,L)/L$ against $1/L$ for fixed β, $\beta = 0.395$, 0.392, 0.390, 0.389, 0.388, 0.387, 0.385, and 0.382 (top to bottom). $L = 10$, 9, 8, 7, 6, 5, 4, and 3 (right to left). Dashed line, estimated criticality, $\beta = 0.3885$.

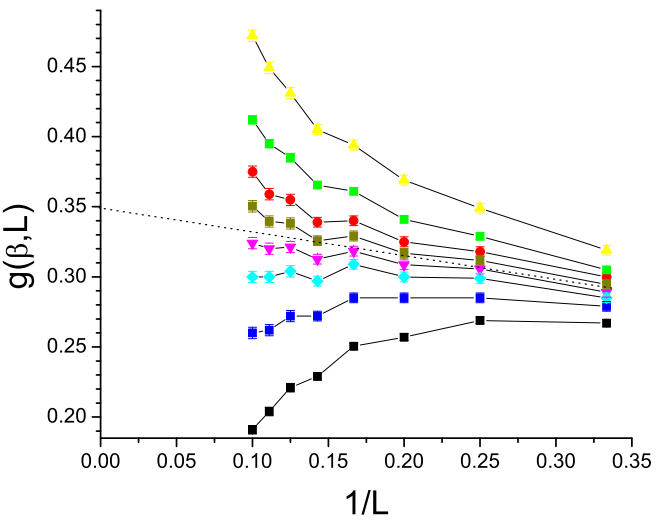

FIG. 11. Bimodal 5D ISG. $g(\beta,L)$ against $1/L$ for fixed β, $\beta = 0.392$, 0.390, 0.389, 0.388, 0.387, 0.385 (top to bottom). $L = 10$, 9, 8, 7, 6, 5, 4, 3 (left to right). Dashed line, estimated criticality, $\beta = 0.3885$.

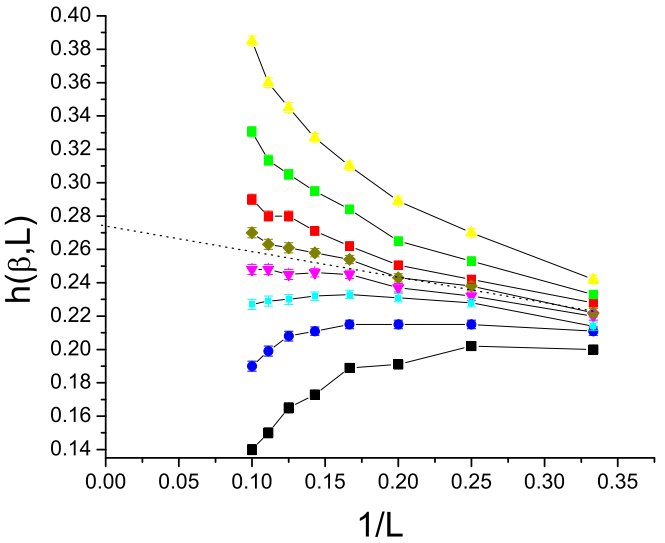

FIG. 12. Bimodal 5D ISG. $h(\beta,L)$ against $1/L$ for fixed β, $\beta = 0.392, 0.390, 0.389, 0.388, 0.387, 0.385$ (top to bottom). $L = 10, 9, 8, 7, 6, 5, 4, 3$ (left to right). Dashed line, estimated criticality, $\beta = 0.3885$.

extrapolation are $\gamma = 1.73(3)$ and $\nu = 0.76(1)$, and the fit curves correspond to the ThL expressions

$$\chi(\tau) = 0.73\tau^{-1.73}(1 + 0.37\tau^{0.95} - 0.005\tau^{8}), \tag{28}$$

$$\xi(\tau) = 0.94\beta\tau^{-0.76}(1 + 0.068\tau). \tag{29}$$

The simulation β_c, γ, and ν values are in excellent agreement with the quite independent HTSE bimodal critical value estimates $\beta_c = 0.389(1)$, $\gamma = 1.73(3)$, and $\nu \approx 0.73$ of Klein *et al* [11] discussed in detail in Sec. XII.

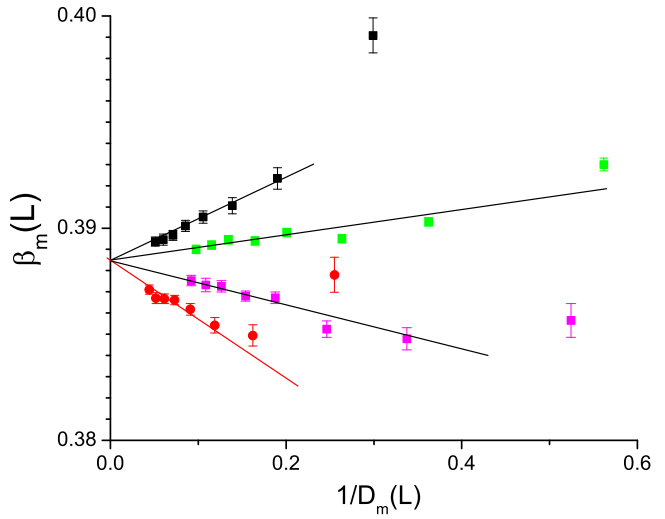

FIG. 13. Bimodal 5D ISG. Peak location $y = \beta_{\max}$ against inverse peak height $x = 1/D_{\max}$ for the derivative sets $\partial h(\beta,L)/\partial\beta$, $\partial P_W(\beta,L)/\partial\beta$, $\partial P_{\text{skew}}(\beta,L)/\partial\beta$, and $\partial g(\beta,L)/\partial\beta$ (top to bottom). Sizes $L = 3, 4, 5, 6, 7, 8, 9$, and 10 (increasing to the left). For each observable the points extrapolate to $y(x) = \beta_c$ at the intercept; see text.

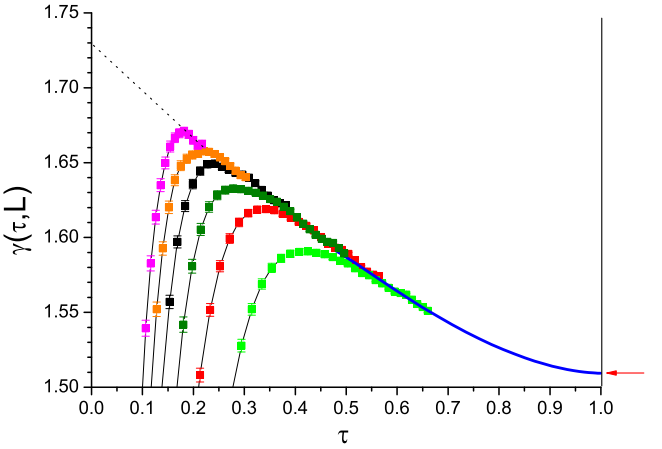

FIG. 14. Bimodal 5D ISG. Effective exponent $\gamma(\tau,L)$ as a function of τ with $\beta_c = 0.3885$. Points, simulation data for $L = 10, 9, 8, 7, 6, 5$ (left to right); continuous (blue) curve on the right, calculated by summing the HTSE tabulation of [12]; dashed line, fit.

A log-log plot of $y(\beta,L) = \chi(\beta,L)/[\xi(\beta,L)/\beta]^2$ against $x(\beta,L) = \xi(\beta,L)/\beta$ is shown in Fig. 16. The estimated limiting slope of the ThL envelope curve $\partial \ln y(\beta,L)/\partial \ln x(\beta,L)$ gives an estimate for the critical exponent $-\eta = 0.28(1)$, without invoking any estimate for β_c. The Privman-Fisher extended scaling plot for $\chi(\beta,L)$ with these critical parameters is shown in Fig. 17.

X. THE 5D UNIFORM DISTRIBUTION ISG MODEL

The numerical data for the uniform distribution model and the Laplacian distribution model are less complete than for the bimodal and Gaussian models because of computing time limitations. Nevertheless, reliable critical parameter estimates have been obtained for both models.

For the uniform distribution model the FSS scaling data for the dimensionless observables $g(\beta,L)$ (Fig. 18), $h(\beta,L)$

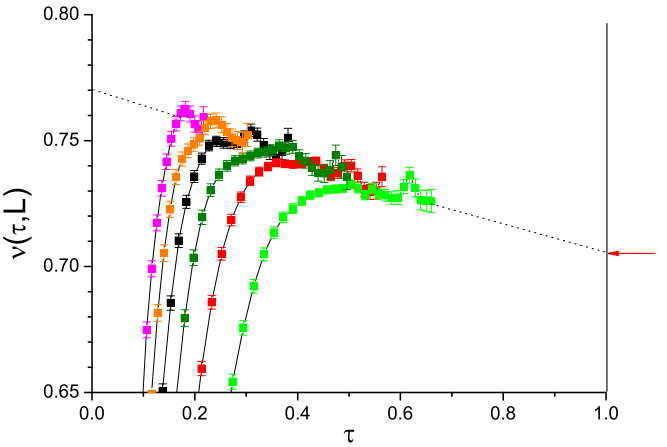

FIG. 15. Bimodal 5D ISG. Effective exponent $\nu(\tau,L)$ as function of τ with $\beta_c = 0.3885$. Points, simulation data for for $L = 10, 9, 8, 7, 6$, and 5 (left to right); red arrow, exact limit; dashed line, fit.

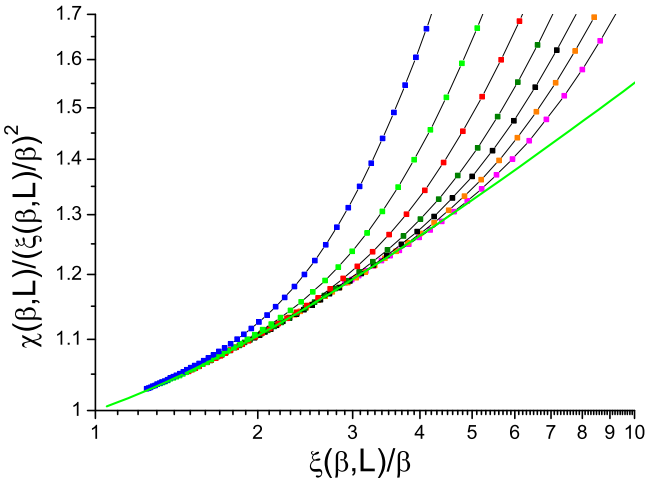

FIG. 16. Bimodal 5D ISG. The ratio $\chi(\beta,L)/[\xi(\beta,L)/\beta]^2$ against $\xi(\beta,L)/\beta$ for $L = 10$, 9, 8, 7, 6, 5, and 4 (right to left). Continuous (green) curve, fit. No value is assumed for β_c.

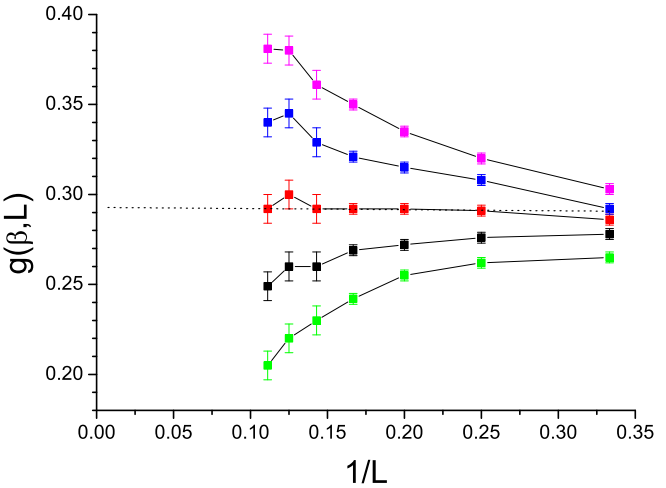

FIG. 18. Uniform 5D ISG. The Binder cumulant $g(\beta,L)$ against $1/L$ for fixed β, $\beta = 0.405$, 0.4025, 0.400, 0.3975, and 0.395 (top to bottom). $L = 9$, 8, 7, 6, 5, 4, and 3 (left to right). Dashed line, estimated criticality, $\beta = 0.400$.

(Fig. 19), $P_W(\beta,L)$, and $W_q(\beta,L)$ all happen to show negligible corrections to scaling and all consistently indicate $\beta_c = 0.400(1)$. The data for the other dimensionless observables show only weak corrections to scaling and are consistent with this β_c. The thermodynamic derivative peak data also confirm the critical temperature value (Fig. 20). The ThL effective exponent fits correspond to

$$\chi(\tau) = 0.93\tau^{-1.625}(1 + 0.104\tau - 0.025\tau^3), \quad (30)$$

$$\xi(\tau) = 0.99\tau^{-0.72}(1 + 0.01\tau^{2.0}), \quad (31)$$

so estimates $\gamma = 1.625(20)$, $\nu = 0.72(1)$, and $\eta = -0.26(3)$ (Figs. 21 and 22). The corrections to scaling are weak. The β_c and γ values can be compared to the HTSE estimates [12] $\beta_c = 0.4016(37)$ and $\gamma = 1.70(15)$. (Here the critical temperature quoted is in terms of the present normalization, not to that used in Ref. [12].) The simulation and HTSE results are consistent, with the wide error bar in the HTSE γ being mainly due to the associated uncertainty in the HTSE β_c^2. A log-log plot of $y(\beta,L) = \chi(\beta,L)/[\xi(\beta,L)/\beta]^2$ against $x(\beta,L) = \xi(\beta,L)/\beta$ is shown in Fig. 23. The limiting slope gives the estimate $-\eta = 0.26(3)$. The Privman-Fisher extended scaling plot for $\chi(\beta,L)$ is shown in Fig. 24. The scaling is excellent until temperatures well below T_c.

XI. THE LAPLACIAN DISTRIBUTION MODEL

For the Laplacian distribution model, the FSS $g(\beta,L)$, $h(\beta,L)$, and $P_W(\beta,L)$ data; see Figs. 25, 26, and 27, respectively. The latter happen to show a negligible correction to

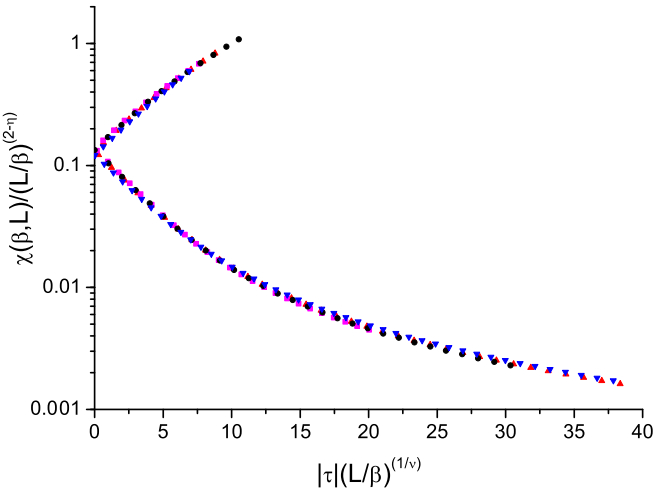

FIG. 17. Bimodal 5D ISG. Privman-Fisher-like scaling of the $\chi(\beta,L)$ data following the form used in [26], with assumed parameters $\beta_c = 0.3885$, $\nu = 0.77$, $\eta = -0.25$ and no adjustments. $L = 10$, pink squares; $L = 8$, black circles; $L = 6$, red triangles; $L = 4$, blue inverted triangles. Upper branch, $\beta > \beta_c$; lower branch, $\beta < \beta_c$.

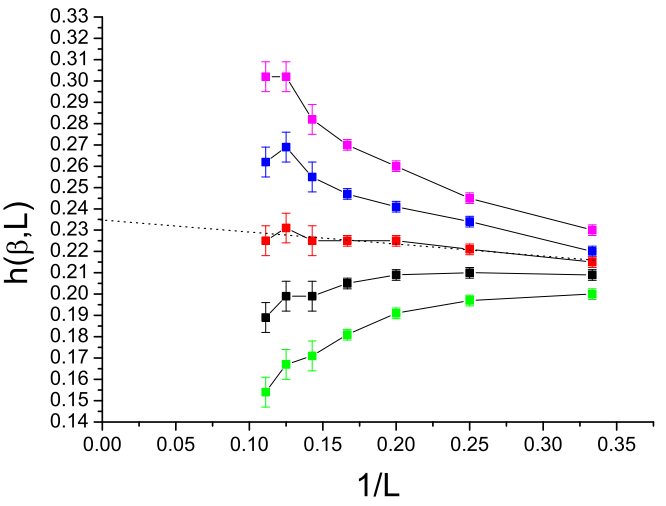

FIG. 19. Uniform 5D ISG. The observable $h(\beta,L)$ against $1/L$ for fixed β, $\beta = 0.405$, 0.4025, 0.4000, 0.3975, 0.3950 (top to bottom). $L = 9$, 8, 7, 6, 5, 4, 3 (left to right). Dashed line, estimated criticality, $\beta = 0.400$.

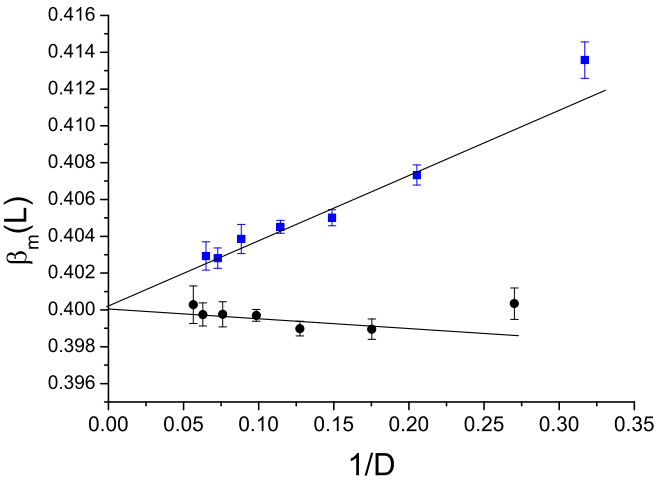

FIG. 20. Uniform 5D ISG. Peak location $y = \beta_{\max}$ against inverse peak height $x = 1/D_{\max}$ for the derivative sets $\partial h(\beta,L)/\partial\beta$ (top) and $\partial g(\beta,L)/\partial\beta$ (bottom). Sizes, $L = 3$, 4, 5, 6, 7, 8, and 9 (increasing to the left). For both observables the points extrapolate to $y(x) = \beta_c$ at the intercept; see text.

scaling, providing an accurate estimate $\beta_c = 0.455(1)$, see Fig. 28. The data for the other dimensionless observables show weak corrections to scaling. Fixed temperature plots of the data (Figs. 25 and 26) are consistent with the same β_c and the critical values of the dimensionless observables given in Table I. The ThL data fits correspond to

$$\chi(\tau) = 1.33\tau^{-1.5}(1 - 0.25\tau^{1.65}), \tag{32}$$

$$\xi(\tau) = 0.973\beta\tau^{-0.69}(1 + 0.028\tau^{2.5}), \tag{33}$$

leading to the critical parameter estimates $\gamma = 1.50(5)$, $\nu = 0.69(2)$, and $\eta = -0.17(3)$, see Figs. 29 and 30. The effective correction exponents are relatively high, indicating a low prefactor for a leading term with $\theta \approx 1.0$.

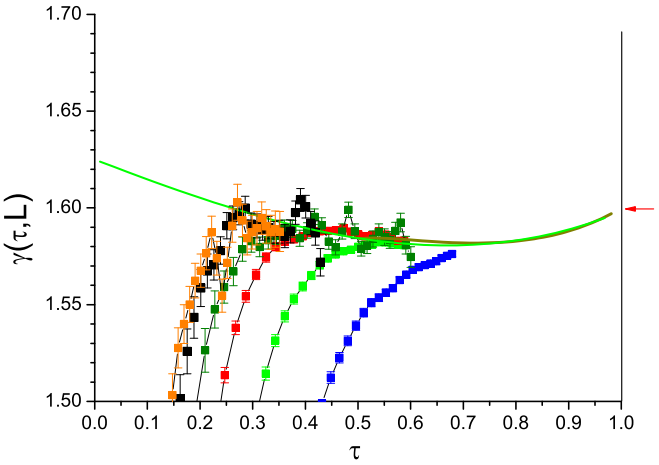

FIG. 21. Uniform 5D ISG. Effective exponent $\gamma(\tau,L)$ as function of τ with $\beta_c = 0.400$. Points, simulation data for $L = 9$, 8, 7, 6, 5, and 4 (left to right). Red arrow, exact limit; continuous (green) curve, fit; continuous (red) curve on the right, almost hidden under the fit curve, calculated by summing the HTSE tabulation of [12].

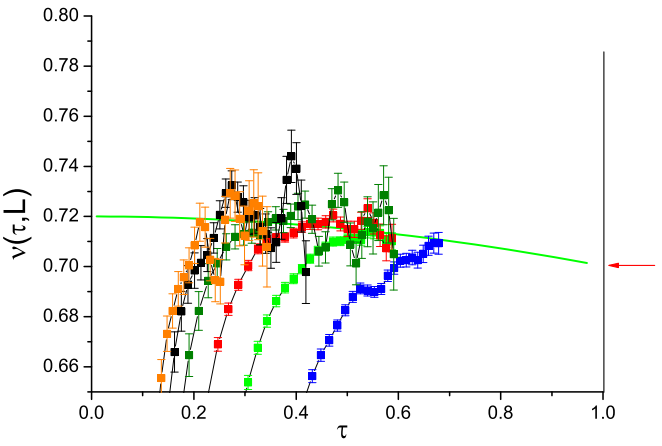

FIG. 22. Uniform 5D ISG. Effective exponent $\nu(\tau,L)$ as function of τ with $\beta_c = 0.400$. Points, simulation data for for $L = 9$, 8, 7, 6, and 5 (left to right). Red arrow, exact limit; continuous (green) curve, fit.

A log-log plot of $y(\beta,L) = \chi(\beta,L)/[\xi(\beta,L)/\beta]^2$ against $x(\beta,L) = \xi(\beta,L)/\beta$ is shownin Fig. 31. The estimated limiting slope of the ThL envelope curve $\partial \ln y(\beta,L)/\partial \ln x(\beta,L)$ gives an estimate for the critical exponent $\eta = -0.19(3)$ without invoking any estimate for β_c. The Privman-Fisher extended scaling for $\chi(\beta,L)$ is shown in Fig. 32. There are no published HTSE data on this model.

XII. HIGH-TEMPERATURE SERIES EXPANSIONS

Having the numerical analyses in hand, we will now discuss in detail the HTSE data [11,12] published some years ago. The HTSE technique is efficient for ISGs in dimension 5 because of the proximity to the ISG upper critical dimension $d = 6$. High-temperature series expansion calculations have been made on the bimodal ISG [11] in general dimension, using $w = \tanh(\beta)^2$ as the scaling variable, and on ISGs with bimodal,

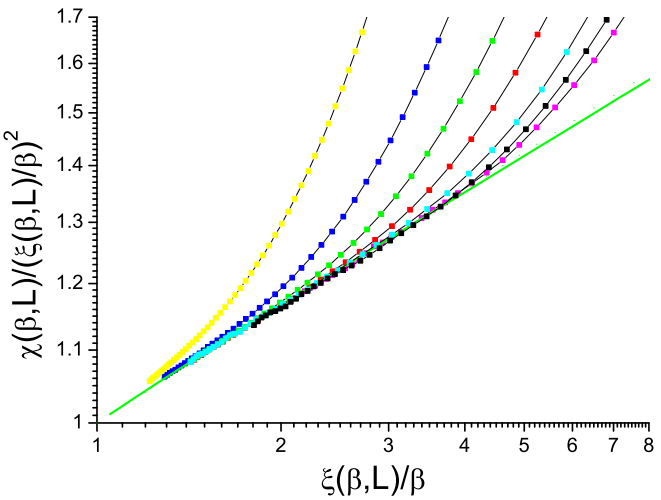

FIG. 23. Uniform 5D ISG. The ratio $\chi(\beta,L)/[\xi(\beta,L)/\beta]^2$ against $\xi(\beta,L)/\beta$ for $L = 9$, 8, 7, 6, 5, 4, and 3 (right to left). Continuous (green) curve, fit. No value is assumed for β_c.

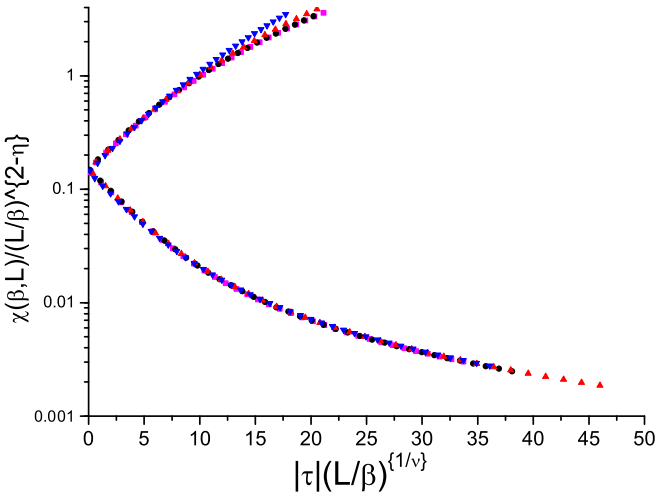

FIG. 24. Uniform 5D ISG. Privman-Fisher-like scaling of the $\chi(\beta,L)$ data following the form used in [26], with assumed parameters $\beta_c = 0.3885$, $\nu = 0.77$, $\eta = -0.25$, and no adjustments. $L = 9$, pink squares; $L = 8$, black circles; $L = 6$, red triangles; $L = 4$, blue inverted triangles. Upper branch, $\beta > \beta_c$; lower branch, $\beta < \beta_c$.

Gaussian, uniform, and double triangle distributions using β^2 as the scaling variable [12], again in general dimension. The number of series terms a_n evaluated was limited by practical considerations to $n = 15$ for bimodal interactions in both cases and to $n = 13$ for the other distributions [12].

In Ref. [12] the spin-glass susceptibility terms were evaluated, and the series were analyzed through Dlog Padé, $M1$ and $M2$ techniques combined with Euler-transformations (see Ref. [12] for details concerning these techniques). The precision on the extrapolations to criticality was limited by the restricted number of terms and by a parasitic antiferromagnetic contribution which oscillates in sign and grows in strength with increasing n. (The Euler transformation is designed to reduce the influence of this parasitic term). The critical β_c^2, the critical

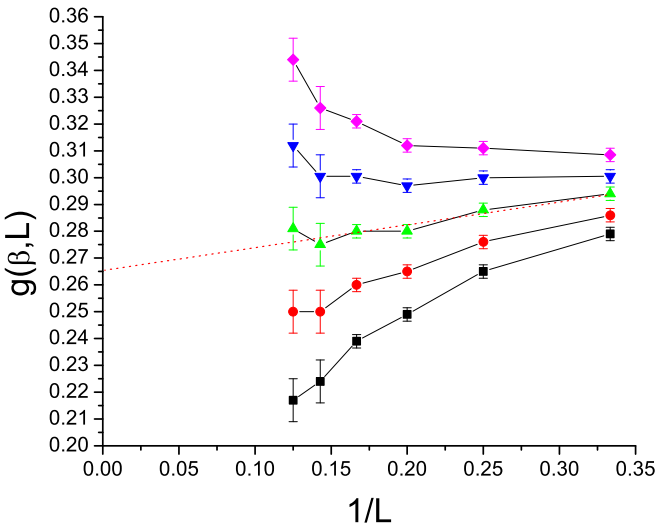

FIG. 25. Laplacian 5D ISG. The parameter $g(\beta,L)$ against $1/L$ for fixed β, $\beta = 0.4600$, 0.4575, 0.4550, 0.4525, 0.4500 (top to bottom). $L = 8$, 7, 6, 5, 4, 3 (left to right). Dashed line, estimated criticality, $\beta = 0.455$.

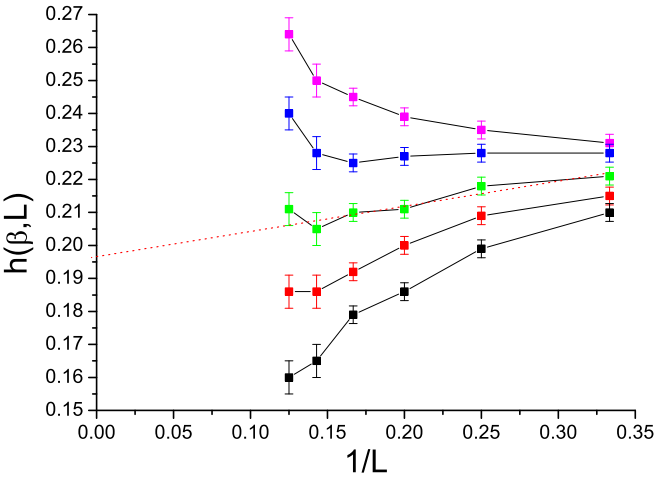

FIG. 26. Laplacian 5D ISG. The parameter $h(\beta,L)$ against $1/L$ for fixed β, $\beta = 0.4600$, 0.4575, 0.4550, 0.4525, 0.4500 (top to bottom). $L = 8$, 7, 6, 5, 4, 3 (left to right). Dashed line, estimated criticality, $\beta = 0.455$.

exponent γ, and the leading correction term exponent θ were evaluated globally using the different analysis techniques. The final estimates for both β_c^2 and γ were cited with rather large error bars. We will concentrate on the Dlog Padé analysis. Including Euler transformations, a large number of individual Dlog Padé solutions were generated for each model. Each individual solution provided precise linked estimates of the critical parameters $[\beta_c^2, \gamma]$. For the 5D Gaussian model explicit point-by-point data were presented in Fig. 7 of Ref. [12], which shows the γ against β_c^2 estimates for each individual solution. The values of the two parameters are highly correlated, with the estimates being fairly dispersed, but with the γ values essentially a smooth function of the β_c^2 values (see inset to Fig. 7 of Ref. [12]). The authors quote as their final Dlog Padé estimates $\beta_c^2 \approx 0.174$ with the associated global estimate $\gamma = 1.67(8)$, and $\beta_c^2 = 0.177(3)$ and 1.75(15) from the other

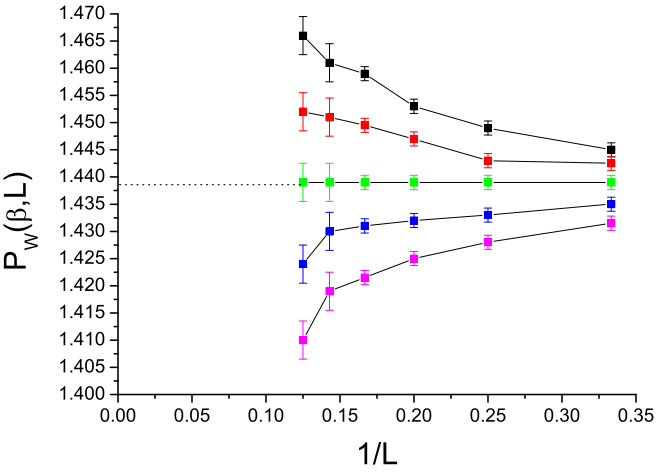

FIG. 27. Laplacian 5D ISG. The parameter $P_W(\beta,L)$ against $1/L$ for fixed β, $\beta = 0.450$, 0.4525, 0.455, 0.4575, and 0.460 (top to bottom). $L = 8, 7, 6, 5, 4$, and 3 (left to right). Dashed line, estimated criticality, $\beta = 0.455$.

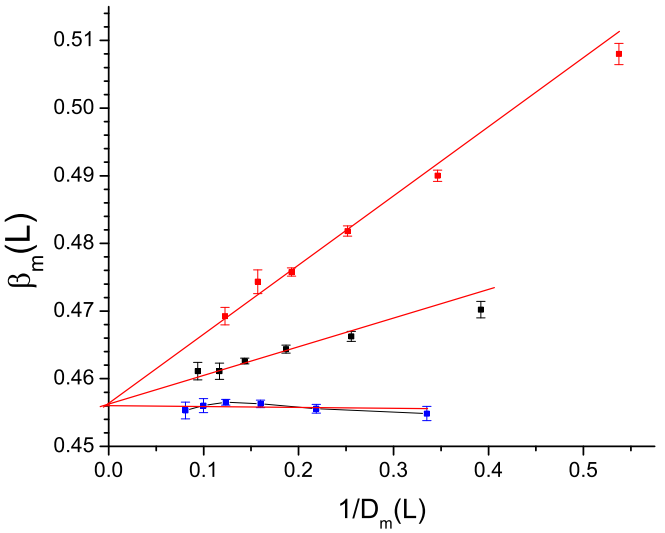

FIG. 28. Laplacian 5D ISG. Peak location $y = \beta_{\max}$ against inverse peak height $x = 1/D_{\max}$ for the derivative sets $\partial W_q(\beta,L)/\partial\beta$, $\partial h(\beta,L)/\partial\beta$, and $\partial g(\beta,L)/\partial\beta$ (top to bottom). Sizes $L = 3$, 4, 5, 6, 7, and 8 (increasing to the left). For each observable, the points extrapolate to $y(x) = \beta_c$ at the intercept; see text.

analyses, together with $\theta \approx 1.0$ from all techniques. Imposing the present accurate simulation estimate $\beta_c^2 = 0.1755(5)$ from FSS and thermodynamic derivative peak analyses onto the Gaussian Dlog-Padé results in the inset to Fig. 7 of [12], one can read off a corresponding "threshold biased" estimate $\gamma = 1.59(2)$. This is in full agreement with the Gaussian model simulation estimate above, $\gamma = 1.60(1)$. Unfortunately no point-by-point Dlog Padé figures equivalent to that for the Gaussian model were presented for the bimodal model or for the uniform model.

For the bimodal model in dimension 5, the HTSE estimates in [12] are $\beta_c^2 = 0.154(3)$, $\gamma = 1.91(10)$ or 1.95(15), again with rather wide error bars. However, the earlier HTSE study by the same group on the bimodal ISG model in general

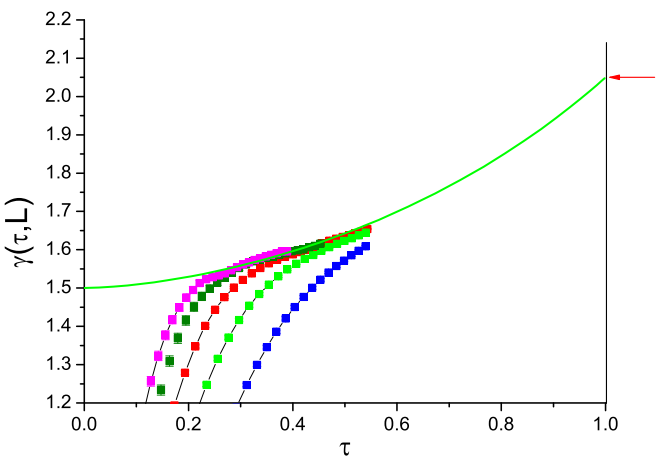

FIG. 29. Laplacian 5D ISG. Effective exponent $\gamma(\tau,L)$ as a function of τ with $\beta_c = 0.455$. Points, simulation data for $L = 8$, 7, 6, 5, and 4 (left to right); red arrow, exact limit; continuous (green) curve, fit.

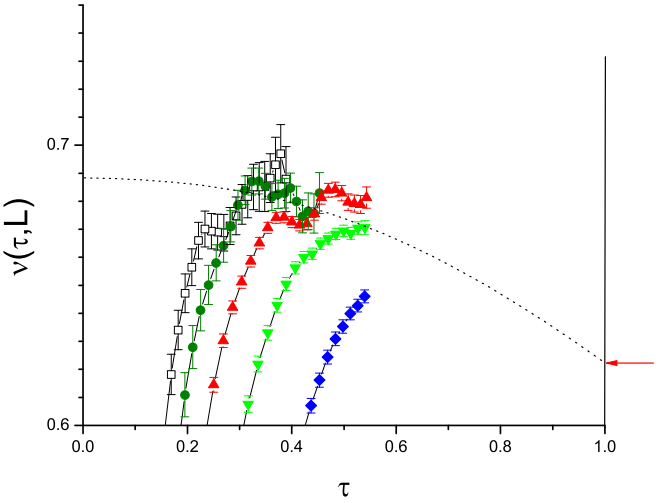

FIG. 30. Laplacian 5D ISG. Effective exponent $\nu(\tau,L)$ as function of τ with $\beta_c = 0.455$. Points, simulation data for for $L = 8$, 7, 6, 5, and 4 (left to right); red arrow, exact limit; continuous (green) curve, fit.

dimension [11] using $w = \tanh(\beta)^2$ as scaling parameter was more complete than that of [12], because, in addition to the series for the spin-glass susceptibility (referred to as Γ_2 in Ref. [11]), series for the two higher-order susceptibilities Γ_3 and Γ_4 (defined in [11]) were also evaluated. The RG critical exponents for these higher-order susceptibilities are $\gamma_3 = (3\gamma + d\nu)/2$ and $\gamma_4 = 2\gamma + d\nu$. We have evaluated explicitly the terms a_n for the different series from the tabulations given in Ref. [11]. It turns out that in dimension 5 the parasitic oscillating terms in the a_n series are much weaker for these higher-order susceptibilities than for the standard ISG susceptibility. Because of the supplementary information from the higher-order susceptibilities, the estimates for the critical temperature and the critical exponents in the dimension 5 bimodal ISG model are much more precise in Ref. [11]

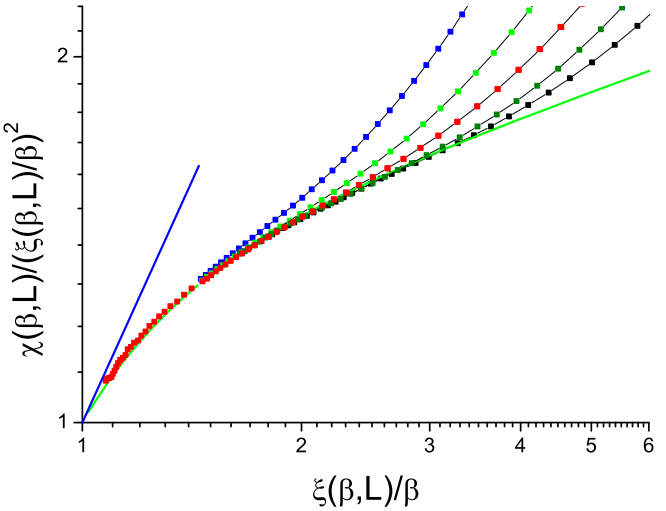

FIG. 31. Laplacian 5D ISG. The ratio $\chi(\beta,L)/[\xi(\beta,L)/\beta]^2$ against $\xi(\beta,L)/\beta$, $L = 8$, 7, 6, 5, and 4 (right to left). Continuous (green) curve, fit. No value is assumed for β_c.

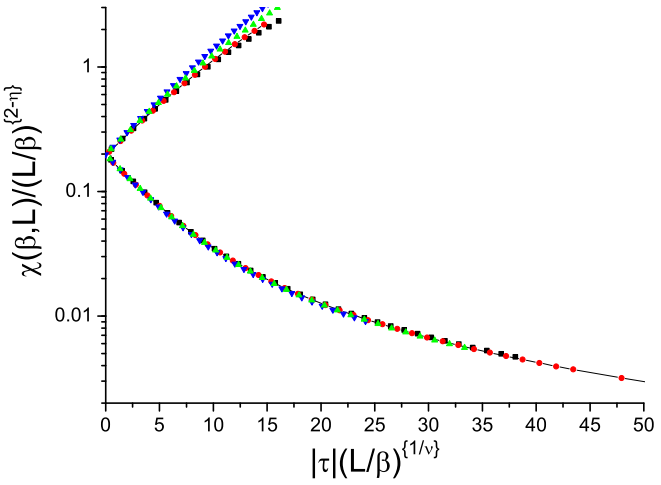

FIG. 32. Laplacian 5D ISG. Privman-Fisher-like scaling of the $\chi(\beta, L)$ data following the form used in [26], with assumed parameters $\beta_c = 0.455$, $\nu = 0.69$, $\eta = -0.21$, and no adjustments. $L = 9$, pink squares; $L = 8$, black squares; $L = 6$, red circles; $L = 5$, green triangles; $L = 4$, blue inverted triangles. Upper branch, $\beta > \beta_c$; lower branch, $\beta < \beta_c$.

than in [12]. The final estimates presented in Ref. [11] are $w_c = 0.1372(8)$, i.e., $\beta_c = 0.389(1)$ or $\beta_c^2 = 0.1513(8)$, and $\gamma = 1.73(3)$, $\gamma_3 = 4.4(1)$, and $\gamma_4 = 7.3(2)$ together with $\theta \approx 1.0$. These values can be compared with the independent values from the simulation estimates given above: $\beta_c = 0.3885(5)$, $\gamma = 1.73(2)$, $\gamma_3 = (3\gamma + d\nu)/2 = 4.5(1)$, $\gamma_4 = 2\gamma + d\nu = 7.3(2)$, and $\theta \approx 1.0$. Remarkably, the present 5D bimodal estimates, based on data obtained from the simulation approach, which is entirely independent technically from HTSE, are in uncanny agreement with the HTSE estimates from 25 yr ago.

For the 5D uniform model the estimates in Ref. [12] are $\beta_c^2 = 0.162(3)$ (with the present normalization) and $\gamma = 1.70(15)$, compatible with but less accurate than the the simulation estimates $\beta_c^2 = 0.160(1)$ and $\gamma = 1.66(2)$. A threshold biased HTSE Dlog Padé estimate for γ would certainly reduce the wide error bar if individual Dlog Padé estimates were available. No HTSE studies have been made of the 5D Laplacian model.

It is important that both Ref. [12] and Ref. [11] estimate the correction exponent in dimension 5 to be $\theta \approx 1.0$ for all models. By definition, there can be correction terms with higher exponents but no correction term with a lower exponent. The corresponding finite-size correction exponent estimate is $\omega = \theta/\nu \approx 1.2$. These HTSE bimodal and threshold biased Gaussian γ estimates [1.73(3) and 1.60(2), respectively] confirm the nonuniversality of 5D ISG critical exponents.

XIII. CONCLUSION

The critical temperatures, critical exponents, and critical values for a number of dimensionless observables have been estimated for the bimodal, Gaussian, uniform, and Laplacian distribution ISG models in dimension 5 from numerical simulations. The values are summarized in Table I.

The accurate ISG inverse ordering temperature β_c values in 5D increase regularly with the kurtosis K of the interaction distribution, in agreement with earlier HTSE estimates and as expected from basic physical arguments [34,35].

More remarkably, the critical exponents also evolve regularly with K. As K increases, the critical exponents γ and ν decrease regularly. Thus, the uniform, Gaussian and Laplacian model γ estimates are approximately 4%, 8%, and 15%, respectively, below the bimodal value. The critical values of the dimensionless parameters also vary if not quite so regularly; the critical dimensionless observable values for the extreme models (bimodal and Laplacian) differ by up to about 30% depending on the observable.

Comparisons are made between the present simulation estimates for the exponent γ in the bimodal and Gaussian models and those obtained independently from HTSE. The most accurate published HTSE bimodal model β_c and γ values [11] and the present simulation estimates are in full agreement, $\beta_c = 0.3885(5)$ and $\gamma = 1.73(3)$. In the Gaussian model, if the present precise simulation value for β_c is used to threshold bias the analysis of the HTSE data [12], the HTSE γ value fully agrees with the simulation estimate. Both techniques then give as the Gaussian model estimate $\gamma = 1.60(2)$, clearly lower than the bimodal model value.

These dimension $d = 5$ ISG data thus confirm the empirical conclusion reached from dimension $d = 4$ and dimension $d = 2$ studies [8–10] that ISG models in a fixed dimension but with different interaction distributions do not lie in the same universality class.

Above the upper critical dimension $d = 6$ the evidence for universality in Ref. [12] is inconclusive, but it appears plausible that the standard universality rules should hold. The parameters for the five-dimensional Ising model are $K = 0$ (there are no outliers in the interaction distribution), with the (mean-field) exponents $\gamma = 1$ and $\nu = 1/2$, which clearly do not respect the ISG trend. However, note that ISGs and ferromagnets are very different. The Ising model has $\langle J_{ij} \rangle = 1$, while the ISG models have symmetric interaction distributions, so $\langle J_{ij} \rangle = 0$. The 5D ISG models are all below the ISG upper critical dimension of 6, while the 5D Ising model is above the Ising upper critical dimension of 4.

One can possibly compare the present ISG data with the exponents for the percolation model, where the upper critical dimension is again 6 and where the critical exponents have been measured accurately. In 5D percolation the major exponents are $\gamma = 1.185(5)$ and $\nu = 0.57(1)$ [36], perhaps indicating values which might be reached for an "infinite kurtosis" limit ISG model.

It is relevant that experimental measurements have already shown clearly that critical exponents in $d = 3$ Heisenberg spin glasses vary considerably from system to system, depending on the strength of the Dzyaloshinsky-Moriya coupling term [37].

ACKNOWLEDGMENTS

The authors wish to thank Ralph Chamberlin, Joes Bijvoet, and Jan Aarts for helpful comments. The computations were performed on resources provided by the Swedish National Infrastructure for Computing (SNIC) at the High Performance

Computing Center North (HPC2N) and Chalmers Centre for Computational Science and Engineering (C3SE).

APPENDIX A: EXTRAPOLATION TO CRITICALITY

The Wegner expression [28] for the temperature variation of the thermodynamic limit [$L \gg \xi(\tau)$] spin glass susceptibility is

$$\chi(\tau) = C_\chi \tau^{-\gamma}(1 + a_\chi \tau^\theta + b_\chi \tau^{\theta'} + \cdots), \qquad \text{(A1)}$$

where $\theta = \nu\omega$ is the leading Wegner correction exponent and the second term is generally supposed to be analytic. In practice, we limit the series to two terms for the data fits, and we have no *a priori* knowledge of the critical exponent γ or of the correction exponents θ and θ'. There is, however, a strict infinite temperature limit $\chi(1) = 1$. The temperature-dependent effective susceptibility exponent is then

$$\gamma(\tau) = \frac{-\partial \ln \chi(\tau)}{\partial \ln \tau} = \gamma - \frac{a_\chi \theta \tau^\theta + b_\chi \theta' \tau^{\theta'}}{1 + a_\chi \tau^\theta + b_\chi \tau^{\theta'}}, \qquad \text{(A2)}$$

with a strict infinite temperature limit $\gamma(1) = 2d\beta_c^2$. As equilibration has been carried out to below T_c and as the ThL data extend down to $T \approx 1.1T_c$ for the largest L, full equilibration can be confidently assumed for the ThL envelope data. The statistical error bars on the numerical data are weak (except for the largest L in the uniform model, where the number of samples is much smaller than elsewhere) and are nonexistant for the high-temperature HTSE data. The agreement between data for different L sets for each model (which are statistically independent) and between the HTSE and simulation data can be noted.

Standard fitting procedures were carried out by first assuming $\theta \approx 1$ and adjusting γ, θ', a_χ, and b_χ so as to optimize the fits, with the infinite-temperature-limit conditions imposed. It was essential in all cases to include a second correction term. The correction prefactors vary considerably from model to model, with the effective a_χ sometimes being negligible. The final error bars quoted on the extrapolated estimate for the critical exponent γ include a residual uncertainty associated with the fitting procedure and an uncertainty associated with the value of the critical inverse temperature β_c. [It can be noted that the standard finite-size scaling procedures for determining the exponent γ in ISGs are not direct but rely on independent estimates for ν and η together with the relation $\gamma = (2 - \eta)\nu$.]

The temperature-dependent effective correlation length exponent is

$$\nu(\tau) = \frac{-\partial \ln[\xi(\tau)/\beta]}{\partial \ln \tau} = \nu - \frac{a_\xi \theta \tau^\theta + b_\xi \theta' \tau^{\theta'}}{1 + a_\xi \tau^\theta + b_\xi \tau^{\theta'}}, \qquad \text{(A3)}$$

with the infinite-temperature-limit conditions $\xi(\tau)/\beta \to 1$ and $\nu(\tau) \to (D - K/3)\beta_c^2$, where K is the kurtosis of the interaction distribution. A similar fitting procedure was applied to the correlation length data as to the susceptibility data. It can be seen in the figures that the effective correlation length exponent data are intrinsically more noisy than the effective susceptibility exponent data but that the correction terms are very weak, so the main contribution to the uncertainty in the extrapolated estimate for the critical exponent ν is purely statistical.

The quality of the Privman-Fisher-like scaling provides an overall validation for the fit parameters for both $\gamma(\tau)$ and $\nu(\tau)$ as these plots englobe all the data, not only data from the ThL limit but also data at temperatures close to (and even below) the critical temperature for all L.

APPENDIX B: DATA QUALITY

The question of intrasample errors was already discussed explicitly in the context of early exchange Monte Carlo measurements in the 3D bimodal ISG model by Ballesteros *et al.* [38], who concluded that with even a modest number of measurement steps the intrasample variance rapidly becomes unimportant as compared with the intersample term. Later work on ISG simulations concentrated rather on the conditions for equilibration [6,39,40]. In the present simulations we make many more measurement steps than Ballesteros *et al.* We have nevertheless made explicit tests concerning the intrasample variance in the 5D bimodal model.

So, recall that, e.g., $\langle |q| \rangle, \langle q^2 \rangle$ for each sample are themselves mean values also having standard errors, i.e., intrasample errors. We compute these quantities in the usual manner, assuming independence of measurements. However, for a 32-sample subset of the samples we stored each individual measurement and estimated their moments of the observables using the bootstrap method in case measurements cannot be treated as independent. We find no significant difference between these bootstrap estimates and the usual moment means. It should be added here that for most temperatures the exchange ratio is at least 30%, which means that the probability of measuring on the same sample twice in a row (for a given temperature) is less than (roughly) 50%, which, of course, is beneficial to the independence between measurements. Regarding equilibration again, neither do moments of observables from the first and second half of the measurements show any significant difference. (This equilibration criterion was used, for instance, in Ref. [41].)

Given a set of samples the standard error of a grand mean (mean of the means) over these particular samples for some observable U is $\hat{\epsilon} = \epsilon_{\text{rms}}/\sqrt{N_s}$, where ϵ_{rms} is the root mean square of $\epsilon_1, \ldots, \epsilon_{N_s}$, the standard errors of the mean observables $\langle U \rangle_1, \ldots, \langle U \rangle_{N_s}$, N_s being the number of samples. The parameter $\hat{\epsilon}$ indicates the reliability of our estimated grand mean were we to repeat the measurements for these particular samples. In contrast, the standard error $\hat{\sigma}$ of the random sample grand mean is defined as the standard deviation of the sample means $\langle U \rangle_1, \ldots, \langle U \rangle_{N_s}$ divided by $\sqrt{N_s}$.

The standard error $\hat{\epsilon}$ is very small compared to the grand mean for our data. For observable q^2 the ratio $\hat{\epsilon}/[\langle q^2 \rangle]$ is less than 10^{-4} for all temperatures. A small $\hat{\epsilon}$ does not necessarily give us a small $\hat{\sigma}$. Experimentation, not only on our 5D ISG data, but also on various random parametrized distributions, suggests instead that increasing the number of measurements to obtain a small $\hat{\epsilon}$ just gives a small variation in $\hat{\sigma}$ between repeated experiments. Indeed, the dependence seems to be linear but we make no claims regarding the slope coefficient. At best then, a small $\hat{\epsilon}$ thus indicates stability between repeated experiments, even for the standard error $\hat{\sigma}$.

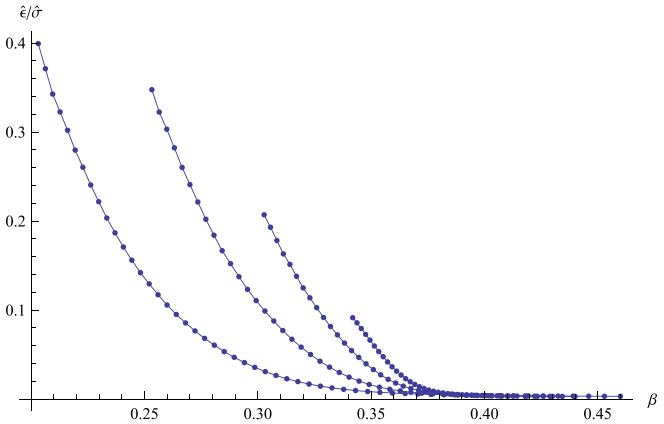

FIG. 33. Bimodal 5D ISG model. The sample specific grand mean standard error $\hat{\epsilon}$ compared to the random sample grand mean standard error $\hat{\sigma}$ for observable q^2, plotted versus inverse temperature β, $L = 4, 6, 8, 10$ (left to right).

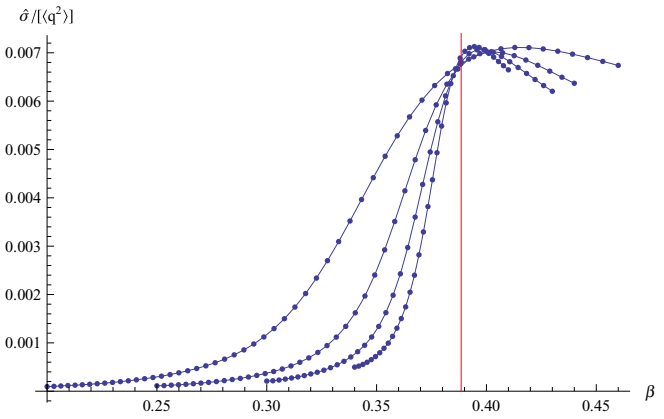

FIG. 34. Bimodal 5D ISG model. The grand mean standard error $\hat{\sigma}$ of observable q^2 for a random sample set compared to its grand mean $[\langle q^2 \rangle]$, plotted versus inverse temperature β, $L = 4, 6, 8, 10$ (left to right). Red line at $\beta_c = 0.3885$.

Our $\hat{\epsilon}$ is, in fact, small when compared to $\hat{\sigma}$, even though the relative error in the observable's grand mean is at its maximum. Figure 33 shows the ratio between the two standard errors $\hat{\epsilon}/\hat{\sigma}$ for observable q^2, and Fig. 34 shows the more relevant standard error $\hat{\sigma}$ in comparison to the grand mean $[\langle q^2 \rangle]$.

To summarize, in agreement with analyses by other groups of exchange Monte Carlo ISG data in dimensions 2, 3, and 4, under standard measurement conditions the influence of intrasample variance can be considered negligible as compared to the intersample variance.

[1] G. Parisi, R. Petronzio, and F. Rosati, Eur. Phys. J. B **21**, 605 (2001).
[2] M. Castellana and G. Parisi, Phys. Rev. E **82**, 040105 (2010).
[3] M. Castellana and G. Parisi, Phys. Rev. E **83**, 041134 (2011).
[4] M. Castellana, Eur. Phys. Lett. **95**, 47014 (2011).
[5] M. C. Angelini, G. Parisi, and F. Ricci-Tersenghi, Phys. Rev. B **87**, 134201 (2013).
[6] M. Hasenbusch, A. Pelissetto, and E. Vicari, Phys. Rev. B **78**, 214205 (2008).
[7] P. Butera and M. Comi, Phys. Rev. B **65**, 144431 (2002).
[8] P. H. Lundow and I. A. Campbell, Phys. Rev. E **91**, 042121 (2015).
[9] P. H. Lundow and I. A. Campbell, Phys. A (Amsterdam, Neth.) **434**, 181 (2015).
[10] P. H. Lundow and I. A. Campbell, Phys. Rev. E **93**, 022119 (2016).
[11] L. Klein, J. Adler, A. Aharony, A. B. Harris, and Y. Meir, Phys. Rev. B **43**, 11249 (1991).
[12] D. Daboul, I. Chang, and A. Aharony, Eur. Phys. J. B **41**, 231 (2004).
[13] E. Gardner, J. Phys. **45**, 1755 (1984).
[14] J. D. van der Waals, Z. Phys. Chem. **13**, 42 (1894).
[15] J. E. Verschaffelt, Versl. Kon. Akad. Wetensch. Amsterdam **8**, 651 (1900).
[16] J. M. H. Levelt-Sengers, Phys. A (Amsterdam, Neth.) **82**, 319 (1976).
[17] L. Onsager, Phys. Rev. **65**, 117 (1944).
[18] K. G. Wilson, Phys. Rev. B **4**, 3174 (1971).
[19] J. S. Kouvel and M. E. Fisher, Phys. Rev. **136**, A1626 (1964).
[20] G. Orkoulas, A. Z. Panagiotopoulos, and M. E. Fisher, Phys. Rev. E **61**, 5930 (2000).
[21] A. M. Ferrenberg and D. P. Landau, Phys. Rev. B **44**, 5081 (1991).
[22] H. G. Katzgraber, M. Palassini, and A. P. Young, Phys. Rev. B **63**, 184422 (2001).
[23] P. H. Lundow and I. A. Campbell, Phys. Rev. B **82**, 024414 (2010).
[24] M. Weigel and W. Janke, Phys. Rev. Lett. **102**, 100601 (2009).
[25] R. R. P. Singh and S. Chakravarty, Phys. Rev. Lett. **57**, 245 (1986).
[26] I. A. Campbell, K. Hukushima, and H. Takayama, Phys. Rev. Lett. **97**, 117202 (2006).
[27] J. G. Darboux, J. Math. Pure Appl. **4**, 377 (1878).
[28] F. Wegner, Phys. Rev. B **5**, 4529 (1972).
[29] I. A. Campbell and P. Butera, Phys. Rev. B **78**, 024435 (2008).
[30] M. E. Fisher and R. J. Burford, Phys. Rev. **156**, 583 (1967).
[31] V. Privman and M. E. Fisher, Phys. Rev. B **30**, 322 (1984).
[32] P. Calabrese, V. Martin-Mayor, A. Pelissetto, and E. Vicari, Phys. Rev. E **68**, 036136 (2003).
[33] K. Hukushima, I. A. Campbell, and H. Takayama, Int. J. Mod. Phys. C **20**, 1313 (2009).
[34] I. A. Campbell, Phys. Rev. B **72**, 092405 (2005).
[35] R. R. P. Singh and M. E. Fisher, J. Appl. Phys. **63**, 3994 (1988).
[36] J. Adler, Y. Meir, A. Aharony, and A. B. Harris, Phys. Rev. B **41**, 9183 (1990).

[37] I. A. Campbell and D. C. M. C. Petit, J. Phys. Soc. Jpn. **79**, 011006 (2010).
[38] H. G. Ballesteros, A. Cruz, L. A. Fernandez, V. Martin-Mayor, J. Pech, J. J. Ruiz-Lorenzo, A. Tarancon, P. Tellez, C. L. Ullod, and C. Ungil, Phys. Rev. B **62**, 14237 (2000).
[39] H. G. Katzgraber, M. Körner, and A. P. Young, Phys. Rev. B **73**, 224432 (2006).
[40] M. Baity-Jesy *et al.*, Phys. Rev. B **88**, 224416 (2013).
[41] T. Jörg and H. G. Katzgraber, Phys. Rev. B **77**, 214426 (2008).